PROCEEDINGS OF SCIENCE

Multiscale VLBI Imaging

Hendrik Müller[a,*] **and Andrei Lobanov**[a]

[a] *Max Planck Institute for Radioastronomy,*
Auf dem Hügel 69, Bonn, Germany

E-mail: hmueller@mpifr-bonn.mpg.de

Reconstructing images from very long baseline interferometry (VLBI) data with sparse sampling of the Fourier domain (uv-coverage) constitutes an ill-posed deconvolution problem. It requires application of robust algorithms maximizing the information extraction from all of the sampled spatial scales and minimizing the influence of the unsampled scales on image quality. We present novel multiscale wavelet deconvolution algorithms for imaging sparsely sampled interferometric data. These new ideas are based on a novel, specially designed wavelet dictionary and hard image thresholding in the spirit of compressive sensing. Compressing various spatial features of the true sky brightness distribution by various scales provides a powerful way to analyse the uv-coverage during imaging and improving the separation between covered features and features introduced by gaps in the uv-coverage. We demonstrate the stability of our novel algorithmic ideas and benchmark their performance against image reconstructions made with CLEAN and Regularized Maximum-Likelihood (RML) methods using synthetic data. The comparison shows that multiscalar approaches match the superresolution achieved by the RML reconstructions and surpass the sensitivity to extended emission reached by CLEAN. Moreover, the imaging is largely data-driven reducing the human induced bias during the imaging procedure. Finally, we present some natural extensions to dynamic imaging, polarimetry and finally dynamic polarimetry.

15th European VLBI Network Mini-Symposium and Users' Meeting (EVN2022)
11-15 July 2022
University College Cork, Ireland

*Speaker

PoS(EVN2022)056

1. Introduction

1.1 VLBI

In Very Long Baseline Interferometry (VLBI) an array of radio telescopes, observing simultaneously a given radio source, is combined in an interferometric mode. The correlation of the recorded signals at any pair of antennas in the array is the Fourier transform of the true sky brightness distribution (visibility) with a Fourier frequency specified by the projected baseline of the antennas as described by the van-Cittert-Zernike theorem [1]:

$$\mathcal{V}(u,v) = \int\int e^{-2\pi i(xu+yv)} I(x,y)dxdy\,, \tag{1}$$

where $\mathcal{V}$ are the observed visibilities at harmonic coordinates (u,v), I is the true sky brightness distribution and x,y projected spatial sky coordinates. The Fourier domain (uv-plane) is only sparsely covered with observations (uv-coverage). The inverse problem, i.e. recovering an image from the observed visibilities, is ill-posed. Additionally thermal noise, and several direction-independent calibration effects culminated in multiplicative, station-based complex gain factors g_i further complicate the problem. The observed visibility on a baseline separating the antennas i,j is therefore [1]:

$$V_{i,j} = g_i g_j^* \mathcal{V}_{i,j} + N_{i,j} \tag{2}$$

1.2 CLEAN

For the past decades CLEAN [2] was the preferred imaging method, mainly because its practicality and its limited demand of computational resources. In CLEAN, the problem is reformulated as a deconvolution problem [2]:

$$I^D = B^D * I, \tag{3}$$

where I^D is the dirty map (the inverse Fourier transform of the sparse observed visibilities) and B^D the dirty beam (the response to an on-sky point source). CLEAN models the image as a set of delta functions: in a first step the location of the maximum in the residual is searched, then a rescaled and shifted dirty beam is substituted from the current residual at this location. These steps are repeated until the final residual is noise-like. The list of delta components is convolved with the clean beam (an approximation to the central peak of the dirty beam) and the last residual is added to the reconstruction. CLEAN allows for manual data visualization and data manipulations strategy: by defining special search windows (CLEAN windows), changing the tapering and weighting schemes of the input visibilities, and self-calibrating the gain solutions alternating with imaging rounds. However, CLEAN has well-known limitations:

- CLEAN introduces a disparity between the model that fits the observed visibilities (list of delta components) and the final image (delta components convolved with the clean beam). This is clearly unphysical as the final images produced by CLEAN do not fit the observed visibilities anymore, e.g. compare the discussion in [3]

- CLEAN does not introduce effective regularization and is therefore prone to overfitting the data, in particular in the gaps of the uv-coverage, e.g. see the discussions in [3]. In fact, the regularization of CLEAN relies on the user finding the correct stopping rule by hand, compare [4].
- CLEAN typically requires supervision by a scientist introducing a significant human bias.
- CLEAN relies on an inverse modeling approach. Hence, the success of CLEAN relies strongly on the success of the phase calibration. A forward modeling approach would be more salient as it allows the direct use of calibration-independent closure quantities [5]. Moro ever, a forward approach would allow straightforwardly to incorporate additional hyperparameters in the reconstruction procedure such as gains, other polarimetric channels or prior distributions [**?**].
- The formal resolution of CLEAN is rigidly set by the precalculated restoring beam. However, recent developements in super-resolution imaging in VLBI demonstrated that the CLEAN beam might be too conservative [6**?** –9]. In fact, the theoretical model fitting resolution of an VLBI array is much higher than the clean beam resolution, but only reachable if the range of possible solutions is limited by strong prior assumptions [10]. Since CLEAN does not make any reasonable prior assumptions compared to Regularized Maximum Likelihood (RML) and Bayesian approaches, its resolution is worse compared to these more recent approaches.
- The representation of the image by a list of CLEAN components is disadvantageous for the reconstruction of extended emission. [11]
- While CLEAN is relatively fast to apply since, after initialization, only subtractions of arrays and list searches have to be applied in the minor loop, it does not scale up well to the data science needs for the next generation of radio interferometers such as the SKA, ngEHT or ngVLA. In particular, CLEAN does not make use of modern GPU accelerated computing infrastructures.

1.3 Forward Modeling

More recently Regularized Maximum Likelihood (RML) methods have been proposed [5, 12–14]. RML methods approach the imaging problem in a forward modeling framework. An objective function, i.e. a weighted sum of data fidelity terms (measuring the fidelity of the fit to the observed data) and regularization term (measuring the feasibility of the solution) is minimized:

$$J(I) = \sum_{\text{data terms}} \alpha_{\mathrm{D}} \chi^2_{\mathrm{D}}(I) + \sum_{\text{regularizers}} \beta_{\mathrm{R}} S_{\mathrm{R}}(I)\,. \tag{4}$$

Here χ^2_D are the data fidelity terms (i.e. the reduced chi^2 to the visibilities, amplitudes, or closure quantities respectively) and S_R the regularization terms (e.g. the l^1 or l^2 norm, a total flux constraint or smoothness promoting total variation and total squared variation terms) balanced by the regularization parameters $\alpha_D, \beta_R \in \mathbb{R}$. RML methods address most of the limitations of CLEAN. They provide accurate reconstruction results, beat CLEAN in terms of resolution, and avoid the disparity between model and image. However, these methods often rely on a number

of non-trivial hyperparameters (the regularization parameters α_D and β_R). In particular for RML methods, this made the use of tedious parameter surveys necessary [6]. An unsupervised alternative would be desired.

2. Multiscale Imaging with DoG-HiT

2.1 Rationale

While for current RML methods a wide range of hyperparameters needs to be evaluated due to the combination of various data and regularization terms, could we step forward towards unsupervised VLBI imaging by making the regularization term more data driven? This is the idea behind DoG-HiT. DoG-HiT approaches the sky brightness distribution with a set of multiscalar basis functions formulated as a dictionary of wavelet functions $\Gamma = \{\Phi_0, \Phi_1, \Phi_2, ...\}$. Γ acts on an array of wavelet coefficients $\mathcal{I} = \{I_0, I_1, ...\}$ (where all I_i are two-dimensional arrays of the size of the true image I) by scale-wise matrix multiplication, i.e. $\Gamma\mathcal{I} = \Phi_0 I_0 + \Phi_1 I_1 + ...$ The Fourier transforms of these wavelets are multiplicative filters in the Fourier domain. Hence, the wavelets can be fitted to the uv-coverage, with some wavelets encoding scalar information of Fourier coefficients that were measured and some wavelets encoding scalar information of Fourier coefficients that were not measured (gaps in the uv-coverage). In this way the wavelet dictionary allows for a separation between observed and not observed scales in the visibility data. For imaging we want to fit the observed visibilities (data-fidelity) with a clean model (i.e. no sidelobes) with the least number of independent model parameters while no image features corresponding to Fourier coefficients in the gaps in the uv-coverage should be induced. Hence, we proposed a compressed sensing approach for DoG-HiT [7]:

$$\hat{\mathcal{I}} \in \mathrm{argmin}_{\mathcal{I}} \left[\chi^2_{\mathrm{cph}}(\Gamma\mathcal{I}, V) + \chi^2_{\mathrm{cla}}(\Gamma\mathcal{I}, V) + \alpha \cdot \|\mathcal{I}\|_{l_0} + R_{\mathrm{flux}}(\mathcal{I}, f) \right], \tag{5}$$

where $\mathcal{I}$ is the array of wavelet coefficients, α is the regularization parameter balancing the data fidelity and sparsity promoting penalization, and R_{flux} is an indicator function total flux constraint for the total flux f. Γ denotes the wavelet dictionary, and as before V the observed visibilities. We use the fit quality to the closure phases χ^2_{cph} and logarithm of closure amplitudes χ^2_{cla} respectively such that the reconstruction is independent from station based gains. As visible from Eq. (5), we compose the image from multiscalar functions that are fitted to the uv-coverage and use a sparsity promoting penalization $\|\cdot\|_{l0}$ penalty term on the wavelet coefficients to suppress any wavelet scales mostly sensitive to the gaps in the uv-coverage.

2.2 Wavelet Dictionary

There are two conflicting requirements for the construction of suitable wavelets. On one hand, the wavelets should be orthogonal and define Heaviside masks in the Fourier domain such that they can be optimally fitted to the uv-coverage. On the other hand, the wavelets should represent the image physically reasonable, i.e. they should smoothly extrapolate into the gaps of the uv-coverage, be free of sidelobes, and contain, if possible, only positive fluxes. In [7] we presented difference of

Gaussian (DoG) wavelet function:

$$\Phi_{\mathrm{DoG}}^{\sigma_1,\sigma_2}(x,y) = \frac{1}{2\pi\sigma_1^2}\exp\left(\frac{-x^2-y^2}{2\sigma_1^2}\right) - \frac{1}{2\pi\sigma_2^2}\exp\left(\frac{-x^2-y^2}{2\sigma_2^2}\right)$$
$$=: G_{\sigma_1} - G_{\sigma_2}, \tag{6}$$

as a plausible approach to construct such wavelets. G_σ denotes here a two-dimensional Gaussian function in the image domain with standard deviation σ. These wavelets have been extended to directional-dependent wavelets by the difference of elliptical Gaussian functions in [3]. An orthogonal set of directional-dependent wavelets was also introduced in [3] using the difference of elliptical Bessel functions (DoB) instead of the difference of elliptical Gaussian functions. The DoG- and DoB-wavelets are related such that the central peak of the DoB-wavelets is approximated by DoG-wavelets. In [3] we proposed a switching scheme between these two different wavelet dictionaries in a CLEAN framework to solve the conflicting requirements for the design of the wavelet functions. By using a standard multiscale CLEAN minor loop with DoB-wavelets as basis functions, we represent the initial residual (dirty image) by a list of DoB-wavelets. Then we replace the DoB-wavelets by DoG-wavelets that approximate the central main lobe of the DoB-wavelets and recompute the residual. Due to a proper selection of the multiscale components, the convolution with a sidelobe-free clean beam (DoG-wavelets) takes place before the residual is updated, and hence the disparity between the image and the model is solved [3].This strategy has been transferred to DoG-HiT in [15]: the decomposition is done with DoB-wavelets, the minimization of Eq. (4) with DoG-wavelets (see also our discussion in Sec. 2.3).

2.3 Imaging Strategy

While in principle Eq. (4) could be minimized directly, more accurate reconstruction were obtained by a multiround imaging pipeline for Stokes I imaging first proposed in [7]. However, the practical application of this approach [9, 16] has revealed the need to refine this imaging strategy as follows:

1. First we find a proper initial guess.

   - We do an unpenalized reconstruction with the software package *ehtim* first, i.e. we use amplitudes, closure phases and closure amplitudes and deactivate any regularization terms except for the total flux regularization. The computed solution I^1 works as an initial guess, but still shows imaging artifacts due to missing regularization.
   - Next we find a multiscale representation of the initial guess. Due to the completeness property DoB-wavelet dictionaries [3], it is a viable parametrization to copy I^1 at every scale, i.e. $\mathcal{I}^1 = \{I^1, I^1, ..., I^1\}$
   - Then we use a grid-search to find an initial guess for the minimization of Eq. (4). The $\|\cdot\|_{l_0}$ penalty term effectively computes a hard thresholding step (proximal-point operator of the l_0-norm). We therefore minimize Eq. (4) on a grid of predefined hard threshold parameters, allowed to vary from scale to scale: $\mathcal{I}^2$

2. Now we do the DoG-HiT imaging step. Up to now DoB-wavelets were used to fit the observed visibilities. Naturally we switch to DoG-wavelets now, as described in [3], by copying the guess $\mathcal{I}^2$, but replacing the dictionary. We then minimize Eq. (4) directly with the forward-backward splitting algorithm developed in [7] and recover the guess image by applying the wavelet dictionary Γ to the array of wavelet coefficients: $I^3 = \Gamma\mathcal{I}^3$.

3. The result can be further refined in alternate imaging and calibration rounds

   - We calibrate the total flux, since the closure quantities are invariant against rescaling array with a constant value. We compute the fit of the guess solution $\Gamma\left[\delta\mathcal{I}^3\right]$ to the amplitudes with a varying constant parameter $\delta \in \mathbb{R}$, peaking around the rescaling parameter δ_{best} that is necessary to reach the correct total flux. Finally, we do phase-self-calibration.
   - As a byproduct of step 2 we get a representation of the multiresolution support [15]. It is expressed as a set of statistically significant wavelet coefficients [see 17, for an application in astrophysical context]. This information is used in further imaging rounds as constrained minimization prior, i.e. we fit the observed visibilities but vary only coefficients in the multiresolution support.
   - We add amplitudes to the array of observables and do imaging starting from $\delta_{\text{best}}I^3$ as an initial guess with the constrained minimization approach with the multiresolution support. After amplitude and phase calibration, we replace closure phases and closure amplitudes by full visibilities and redo the minimization.

2.4 Dynamic Polarimetry

DoG-HiT has been extended to polarimetric and dynamic imaging [9, 15]. The multiresolution support computed from the static, time-averaged Stokes I image by DoG-HiT is a strong prior information for polarimetry and dynamic imaging. It compresses information about the uv-coverage: the multiresolution support specifies where emission is located (support constraint) and which spatial scales are significant to represent these features (multiscalar constraint). This prior information is useful for polarimetry since all Stokes parameters have the same uv-coverage (multiscalar constraint) and the fraction of linear and circular polarization is always smaller than one (support constraint). Moreover, the same set of prior information is also desired for dynamic imaging as the uv-coverage of the complete observation run is the sum of the much sparser uv-coverages of the single scans. Hence, DoG-HiT is able to provide dynamic movie reconstructions and polarimetric images as well with the same strategy that was used to refine the Stokes I images: fitting the (polarimetric) visibilities scan by scan in a constrained minimization scheme, i.e. by only varying the coefficients in the multiresolution support.

3. Conclusions

We benchmarked the performance of multiscale imaging (DoB-CLEAN variant of DoG-HiT) against CLEAN in [7], see also Fig. 1. DoG-HiT performs better than CLEAN in terms of accuracy and resolution. Moreover, DoG-HiT introduces an effective regularization through its

sparsity promoting regularization approach and solves the disparity between a model and a final image necessarily inherent to CLEAN reconstructions. Furthermore, we demonstrated in [3] that multiscale and multidirectional wavelet sparsity approaches (such as DoB-CLEAN and DoG-HiT) also have the potential to outperform CLEAN and classical MS-CLEAN [11] in terms of wide-field imaging, i.e. in the uniform representation of extended emission. Hence, DoG-HiT effectively deals with the most notorious limitations of CLEAN.

DoG-HiT presents a significant step towards unsupervised imaging. Since the regularization term (sparsity of wavelet coefficients of a wavelet dictionary fitted to the uv-coverage) is data-driven and chosen completely automatically, there is only one free parameter in the objective functional (the regularization parameter α), thus making extended parameter surveys needless. Moreover, benchmarking of DoG-HiT against state-of-the-art imaging RML methods demonstrates that DoG-HiT allows for reconstructions of the same quality (resolution) or sometimes even better quality than RML methods (extended emission, dynamic range), although the regularizer landscape is considerably simpler. DoG-HiT requires the evaluation of a fast Fourier transform and an application of multiscalar dictionary at every iteration. Since the wavelet dictionary has to be allocated only once before the iterations start and the evaluation of the wavelet dictionary is only a matrix-array operation, DoG-HiT remains comparable fast to RML methods, significantly outperforming CLEAN.

DoG-HiT provides the multiresolution support as a byproduct and this has been proven beneficial in the reconstruction of dynamic movies and polarimetric images [7, 15]. Hence, in a straightforward manner DoG-HiT can also recover polarimetric movies without the introduction of any additional regularization or temporal correlation terms. Thus, for these applications DoG-HiT remains largely unsupervised despite the increased complexity of the reconstruction problem.

DoG-HiT is in active use for a wide range of ongoing (polarimetric) mm-VLBI projects such as observations of 3C279, OJ287 and CenA with the EHT in 2017, or observations of 3C279 with the GMVA in 2018 [18]. Moreover, it has been applied to lower frequencies for observations of M87 with RadioAstron [16]. Furthermore, an application to the complete MOJAVE archive of 3C120 demonstrated convincingly the potential of DoG-HiT for survey observations: we were able to reanalyze $\sim$ 100 epochs in roughly $\sim$ 15 minutes with the highly parallelized and fully automated DoG-HiT algorithm and obtained images at higher resolution and comparable dynamic range [18]. Based on the success of DoG-HiT in this variety of observations, we expect great improvements for EVN images. In particular, we expect improvements for combined EVN+eMerlin observations since the wide range of accessible baselines (short baselines from eMerlin combined together with the global baselines of the EVN) makes the use of a multiscalar algorithm that recovers large scale structures and small scale structures in parallel necessary. This benefit is studied in particular in an ongoing study of the Crab Nebula observed with the EVN+eMerlin array in 2022.

DoG-HiT and its extensions are publicly available as part of the *MrBeam* software package under the url: `https://github.com/hmuellergoe/mrbeam`.

References

[1] A. Thompson, J. Moran, and G. Swenson, *Interferometry and Synthesis in Radio Astronomy*. Krieger Publishing Company, 1994.

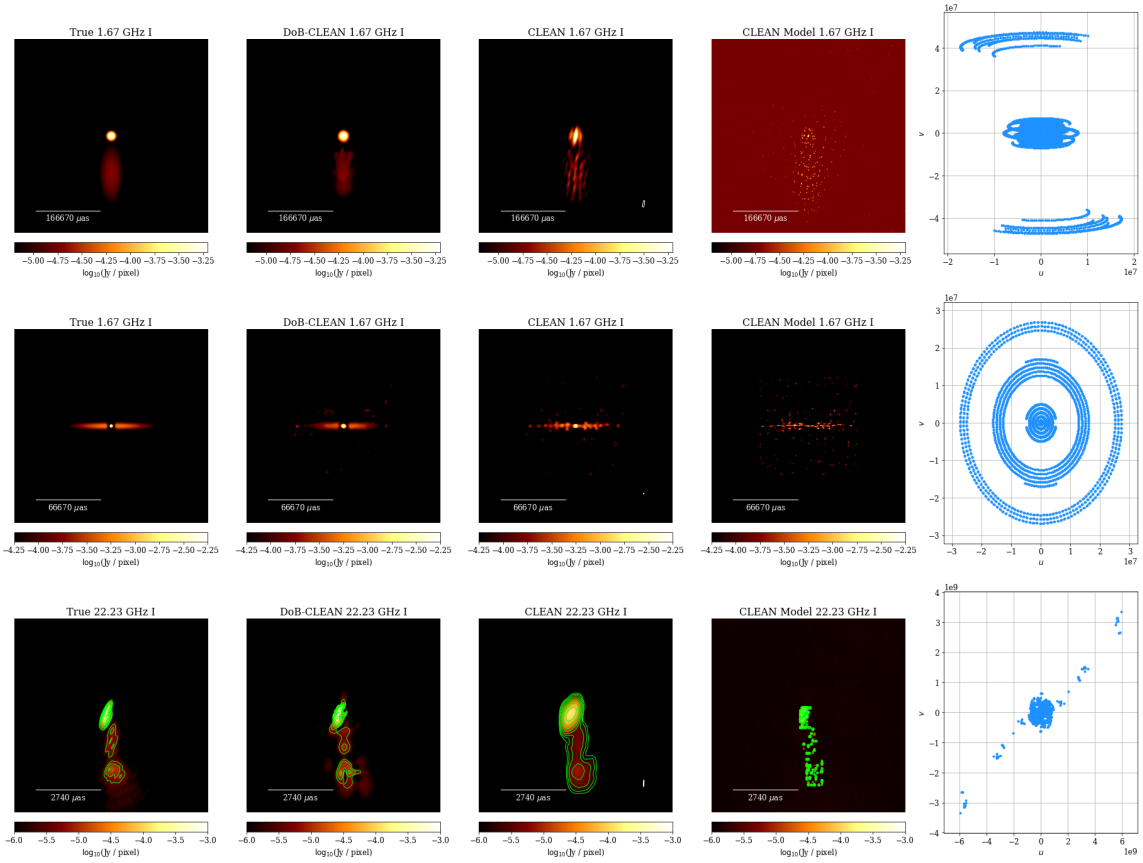

Figure 1: Comparison of a multiscale imaging routine (DoB-CLEAN variant of DoG-HiT) and CLEAN reconstructions on synthetic data, adapted from [3].

[2] J. A. Högbom, *Aperture Synthesis with a Non-Regular Distribution of Interferometer Baselines*, *AAPS* **15** (June, 1974) 417.

[3] H. Müller and A. P. Lobanov, *Multiscale and multidirectional very long baseline interferometry imaging with CLEAN*, *A&A* **672** (Apr., 2023) A26, [2301.11681].

[4] U. J. Schwarz, *Mathematical-statistical Description of the Iterative Beam Removing Technique (Method CLEAN)*, *A&A* **65** (Apr., 1978) 345.

[5] A. A. Chael, M. D. Johnson, K. L. Bouman, L. L. Blackburn, K. Akiyama, and R. Narayan, *Interferometric Imaging Directly with Closure Phases and Closure Amplitudes*, *ApJ* **857** (Apr., 2018) 23, [1803.07088].

[6] Event Horizon Telescope Collaboration, *First M87 Event Horizon Telescope Results. IV. Imaging the Central Supermassive Black Hole*, *ApJL* **875** (Apr., 2019) L4, [1906.11241].

[7] H. Müller and A. P. Lobanov, *DoG-HiT: A novel VLBI multiscale imaging approach*, *A&A* **666** (Oct., 2022) A137, [2206.09501].

[8] A. E. Broderick, D. W. Pesce, R. Gold, P. Tiede, H.-Y. Pu, R. Anantua, S. Britzen, C. Ceccobello, K. Chatterjee, Y. Chen, N. S. Conroy, G. B. Crew, A. Cruz-Osorio, Y. Cui, S. S. Doeleman, R. Emami, J. Farah, C. M. Fromm, P. Galison, B. Georgiev, L. C. Ho, D. J. James, B. Jeter, A. Jimenez-Rosales, J. Y. Koay, C. Kramer, T. P. Krichbaum, S.-S. Lee, M. Lindqvist, I. Martí-Vidal, K. M. Menten, Y. Mizuno, J. M. Moran, M. Moscibrodzka, A. Nathanail, J. Neilsen, C. Ni, J. Park, V. Piétu, L. Rezzolla, A. Ricarte, B. Ripperda, L. Shao, F. Tazaki, K. Toma, P. Torne, J. Weintroub, M. Wielgus, F. Yuan, S.-S. Zhao, and S. Zhang, *The Photon Ring in M87**, *ApJ* **935** (Aug., 2022) 61, [2208.09004].

[9] F. Roelofs, L. Blackburn, G. Lindahl, S. S. Doeleman, M. D. Johnson, P. Arras, K. Chatterjee, R. Emami, C. Fromm, A. Fuentes, J. Knollmüller, N. Kosogorov, H. Müller, N. Patel, A. Raymond, P. Tiede, E. Traianou, and J. Vega, *The ngEHT Analysis Challenges*, *Galaxies* **11** (Jan., 2023) 12, [2212.11355].

[10] A. P. Lobanov, *Resolution limits in astronomical images*, *arXiv e-prints* (Mar., 2005) astro–ph/0503225, [astro-ph/0503225].

[11] T. J. Cornwell, *Multiscale CLEAN Deconvolution of Radio Synthesis Images*, *IEEE Journal of Selected Topics in Signal Processing* **2** (Nov., 2008) 793–801.

[12] K. Akiyama, K. Kuramochi, S. Ikeda, V. L. Fish, F. Tazaki, M. Honma, S. S. Doeleman, A. E. Broderick, J. Dexter, M. Mościbrodzka, K. L. Bouman, A. A. Chael, and M. Zaizen, *Imaging the Schwarzschild-radius-scale Structure of M87 with the Event Horizon Telescope Using Sparse Modeling*, *ApJ* **838** (Mar., 2017) 1, [1702.07361].

[13] K. Akiyama, S. Ikeda, M. Pleau, V. L. Fish, F. Tazaki, K. Kuramochi, A. E. Broderick, J. Dexter, M. Mościbrodzka, M. Gowanlock, M. Honma, and S. S. Doeleman, *Superresolution Full-polarimetric Imaging for Radio Interferometry with Sparse Modeling*, *AJ* **153** (Apr., 2017) 159, [1702.00424].

[14] A. A. Chael, M. D. Johnson, R. Narayan, S. S. Doeleman, J. F. C. Wardle, and K. L. Bouman, *High-resolution Linear Polarimetric Imaging for the Event Horizon Telescope*, *ApJ* **829** (Sept., 2016) 11, [1605.06156].

[15] H. Müller and A. Lobanov, *Dynamic and polarimetric VLBI imaging with a multiscalar approach*, *accepted for publication in A&A, arXiv e-prints* (Mar., 2023) arXiv:2303.11877, [2303.11877].

[16] J.-Y. Kim, T. Savolainen, P. Voitsik, E. V. Kravchenko, M. M. Lisakov, Y. Y. Kovalev, H. Müller, A. P. Lobanov, K. V. Sokolovsky, G. Bruni, P. G. Edwards, C. Reynolds, U. Bach, L. I. Gurvits, T. P. Krichbaum, K. Hada, M. Giroletti, M. Orienti, J. M. Anderson, S.-S. Lee, B. W. Sohn, and J. A. Zensus, *RadioAstron Space VLBI Imaging of the jet in M87: I. Detection of high brightness temperature at 22 GHz, accepted for publication in ApJ, arXiv e-prints* (Apr., 2023) arXiv:2304.09816, [2304.09816].

[17] F. Mertens and A. Lobanov, *Wavelet-based decomposition and analysis of structural patterns in astronomical images*, *AAP* **574** (Feb., 2015) A67, [1410.3732].

[18] H. Müller, *Advanced VLBI Imaging*. PhD thesis, University of Cologne, submitted.